**Proceedings of the ASME 2007 International Design Engineering Technical Conferences & Computers and Information in Engineering Conference**
**IDETC/CIE 2007**
**September 4-7, 2007, Las Vegas, Nevada, USA**

# DETC2007/PTG-34077

# DYNAMIC INTERACTIONS BETWEEN SLIDING FRICTION AND TIP RELIEF IN SPUR GEARS

**Song He**
Acoustics and Dynamics Laboratory
The Ohio State University
Columbus, OH 43210
he.81@osu.edu

**Rajendra Singh***
Acoustics and Dynamics Laboratory
The Ohio State University
Columbus, OH 43210
singh.3@osu.edu

## ABSTRACT
The chief objective of this article is to examine dynamic interactions between sliding friction and profile modifications in a spur gear pair. First, a new computational method is proposed that incorporates the sliding friction and realistic time-varying stiffness into a multi-degree-of-freedom system model. Second, competing friction formulations, such as the Coulomb dry friction model and empirical expressions based on elasto-hydrodynamic and/or boundary lubrication regime principles, are briefly evaluated and validated by comparing friction force predictions with measurements. Third, effect of the profile modification on the dynamic transmission error is analytically examined under the influence of sliding friction. An out-of-phase relationship between the normal load and friction force is found to be critical as it could amplify motions or forces in the off-line-of-action direction. Typical tip relief schemes are examined including the perfect involute profile (baseline), short tip relief (at light load), intermediate tip relief (at medium load) and long tip relief (at peak load). Case studies are evaluated over a range of operating loads; interactions between sliding friction and profile modifications are observed. Finally, principles that could minimize dynamic transmission errors in the presence of sliding friction are introduced.

## 1 INTRODUCTION
In a series of articles, Vaishya and Singh [1-3] developed a spur gear pair model with periodic tooth stiffness variations and sliding friction based on the assumption that load is equally shared among all the teeth in contact. While the assumption of equal load sharing yields simplified expressions and analytically tractable solutions, it may not lead to a realistic model. Houser et al. [4] experimentally demonstrated that the friction forces play a pivotal role in determining the load transmitted to the bearings and housing in the off-line-of-action (OLOA) direction. Velex and Cahouet [5] described an iterative procedure to evaluate the effects of sliding friction, tooth shape deviations and time-varying mesh stiffness in spur and helical gears and compared simulated bearing forces with measurements. Velex and Sainsot [6] analytically found that the Coulomb friction should be viewed as a non-negligible excitation source to error-less spur and helical gear pairs, especially for translational vibrations and high contact ratio gears. Lundvall et al. [7] considered profile modifications and manufacturing errors in a spur gear model and examined the effect of sliding friction on the angular dynamic motions. Recently, He et al. [8] proposed a multi degree-of-freedom (MDOF) spur gear model with realistic mesh stiffness and Coulomb friction. This paper is an extension of [8] to study the effect of time-varying friction coefficient and to quantify dynamic interactions between the sliding friction and mesh stiffness for a gear pair with tip relief.

## 2 MDOF SYSTEM FORMULATION
Transitions in key meshing events within a mesh cycle are determined from the undeformed gear geometry. Figure 1(a) is a snapshot for the example gear set (contact ratio $\sigma = 1.6$) at the beginning ($t = 0$) of the mesh cycle ($t_c$). At that time, pair # 1 (defined as the tooth pair rolling along line AC) just comes into mesh at point A and pair # 0 (the tooth pair rolling along line CD) is in contact at point C, which is the highest point of single tooth contact (HPSTC). When pair #1 approaches the lowest point of single tooth contact (LPSTC) at point B, pair # 0 leaves contact. Further, when pair #1 passes through the pitch point P, the relative sliding velocity of the pinion with respect to the gear is reversed, resulting in a reversal of the friction force. Beyond point C, pair # 1 is re-defined as pair # 0 and the incoming pair at point A is re-defined as pair # 1; this results in a linear-time-varying (LTV) formulation. Figure 1(b) shows the spur gear pair model with the following key assumptions: (i) pinion and gear are rigid disks; (ii) shaft-bearings stiffness elements in the line-of-action (LOA) and OLOA directions are modeled as lumped springs which are connected to a rigid casing; (iii) vibratory angular motions are small in comparison to the kinematic motion.

* Author of correspondence, Phone: (614) 292-9044, Fax: (614) 292-3163.

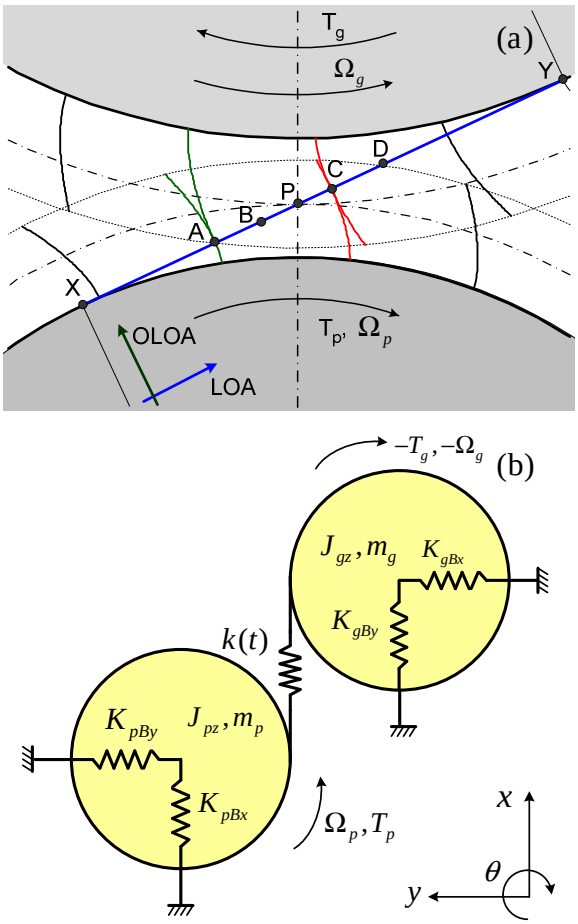


**Figure 1:** (a) Snap shot of contact pattern (at $t$ = 0) in the spur gear pair; (b) MDOF model of spur gear pair; here $k(t)$ is in the LOA direction.

Overall, we obtain a linear time-varying (LTV) system formulation [8] with a constant coefficient of friction $\mu$. Next, we refine the MDOF model of Fig. 1 and consider time-varying sliding friction $\mu(t)$. The resulting governing equations for the torsional motions $\theta_p(t)$ and $\theta_g(t)$ are:

$$J_p\ddot{\theta}_p(t) = T_p + \sum_{i=0}^{n=\text{floor}(\sigma)} X_{pi}(t)\cdot F_{pfi}(t) - \sum_{i=0}^{n=\text{floor}(\sigma)} r_{bp}\cdot N_{pi}(t) \quad (1)$$

$$J_g\ddot{\theta}_g(t) = -T_g + \sum_{i=0}^{n=\text{floor}(\sigma)} X_{gi}(t)\cdot F_{gfi}(t) + \sum_{i=0}^{n=\text{floor}(\sigma)} r_{bg}\cdot N_{gi}(t) \quad (2)$$

Here, the "floor" function rounds off the contact ratio $\sigma$ to the nearest integer (towards a lower value); $J_p$ and $J_g$ are the polar moments of inertia for the pinion and gear; $T_p$ and $T_g$ are the external and braking torques; $N_{pi}(t)$ and $N_{gi}(t)$ are the normal loads defined as follows:

$$N_{pi}(t) = N_{gi}(t) = k_i(t)\left[r_{bp}\cdot\theta_p(t) - r_{bg}\cdot\theta_g(t) + x_p(t) - x_g(t)\right]$$
$$+c_i(t)\left[r_{bp}\cdot\dot{\theta}_p(t) - r_{bg}\cdot\dot{\theta}_g(t) + \dot{x}_p(t) - \dot{x}_g(t)\right]$$
$$i = 0,1,\ \ldots,\ n = \text{floor}(\sigma) \quad (3)$$

where $k_i(t)$ and $c_i(t)$ are the time-varying realistic mesh stiffness and viscous damping profiles; $r_{bp}$ and $r_{bg}$ are the base radii of the pinion and gear; $x_p(t)$ and $x_g(t)$ denote the translational displacements (in the LOA direction) at the bearings. The sliding (interfacial) friction forces $F_{pfi}(t)$ and $F_{gfi}(t)$ of the $i^{th}$ meshing pair are derived as follows:

$$F_{pfi}(t) = \mu(t)N_{pi}(t),\ F_{gfi}(t) = \mu(t)N_{gi}(t)\ \ i = 0\ \ldots n \quad (4a,b)$$

The frictional moment arms $X_{pi}(t)$ and $X_{gi}(t)$ acting on the $i^{th}$ tooth pair are:

$$X_{pi}(t) = L_{XA} + (n-i)\lambda + \text{mod}(\Omega_p r_{bp} t, \lambda),\ \ i = 0,\ \ldots,\ n \quad (5a)$$

$$X_{gi}(t) = L_{YC} + i\lambda - \text{mod}(\Omega_g r_{bg} t, \lambda),\ \ i = 0,\ \ldots,\ n \quad (5b)$$

where "mod" is the modulus function defined as: $\text{mod}(x, y) = x - y\cdot\text{floor}(x/y)$, if $y \neq 0$; "sgn" is the sign function; $\Omega_p$ and $\Omega_g$ are the nominal operational speeds (in rad/s); and $\lambda$ is the base pitch. Refer to Fig. 1(a) for length $L_{AP}$. The governing equations for the translational motions $x_p(t)$ and $x_g(t)$ in the LOA direction are:

$$m_p\ddot{x}_p(t) + 2\zeta_{pBx}\sqrt{K_{pBx}m_p}\,\dot{x}_p(t) + K_{pBx}x_p(t) + \sum_{i=0}^{n=\text{floor}(\sigma)} N_{pi}(t) = 0$$

$$m_g\ddot{x}_g(t) + 2\zeta_{gBx}\sqrt{K_{gBx}m_g}\,\dot{x}_g(t) + K_{gBx}x_g(t) + \sum_{i=0}^{n=\text{floor}(\sigma)} N_{gi}(t) = 0 \quad (6,7)$$

Here, $m_p$ and $m_g$ are the masses of the pinion and gear; $K_{pBx}$ and $K_{gBx}$ are the effective shaft-bearing stiffness values in the LOA direction, and $\zeta_{pBx}$ and $\zeta_{gBx}$ are their damping ratios. Likewise, the governing equations for the translational motions $y_p(t)$ and $y_g(t)$ in the OLOA direction are written as:

$$m_p\ddot{y}_p(t) + 2\zeta_{pBy}\sqrt{K_{pBy}m_p}\,\dot{y}_p(t) + K_{pBy}y_p(t) - \sum_{i=0}^{n=\text{floor}(\sigma)} F_{pfi}(t) = 0$$

$$m_g\ddot{y}_g(t) + 2\zeta_{gBy}\sqrt{K_{gBy}m_g}\,\dot{y}_g(t) + K_{gBy}y_g(t) - \sum_{i=0}^{n=\text{floor}(\sigma)} F_{gfi}(t) = 0 \quad (8,9)$$

## 3 ALTERNATE DYNAMIC FRICTION MODELS

Next, four dynamic friction coefficient models are evaluated and validated [15] using the MDOF spur gear pair model [8] with realistic mesh stiffness profiles.

Gear dynamic researchers [1-7] have typically modeled sliding friction phenomenon by assuming Coulomb formulation with a constant coefficient ($\mu$) of friction (designated here as Model I). Thus the time-varying (periodic) coefficient of friction $\mu_{Ci}(t)$ for the $i^{th}$ meshing tooth pair is derived as follows, where $\mu_{avg}$ is the time-averaged magnitude.

$$\mu_{Ci}(t) = \mu_{avg}\cdot\text{sgn}\left[\text{mod}(\Omega_p r_{bp} t, \lambda) + (n-i)\lambda - L_{AP}\right] \quad (10)$$
$$i = 0\ \ldots n.$$

In reality, tribological conditions change continuously due to varying mesh properties and lubricant film thickness as the gears roll through a full cycle [9-15]. Thus, $\mu$ varies instantaneously with the spatial position of each tooth and the direction of friction force changes at the pitch point. Alternate tribological theories, such as elasto-hydrodynamic lubrication (EHL), boundary lubrication or mixed regime, have been employed to explain the interfacial friction in gears [9-15]. For instance, Benedict and Kelley [9] proposed an empirical

dynamic friction coefficient (designated as Model II) under mixed lubrication regime based on measurements on a roller test machine. The following $\mu(t)$ prediction for the $i^{th}$ meshing tooth pair is based on the Benedict and Kelley model [9], though it is modified to incorporate a reversal in the direction of friction force at the pitch point.

$$\mu_{Bi}(t) = \frac{0.0127\times 1.13}{1.13 - S_{avg}} \log_{10}\left[\frac{29700 w_n}{\eta_M v_{si}(t) v_{ei}^2(t)}\right] \quad i = 0, \ \ldots, \ n$$
$$\cdot \mathrm{sgn}\left[\mathrm{mod}(\Omega_p r_{bp} t, \lambda) + (n-i)\lambda - L_{AP}\right] \tag{11}$$

where $v_{s,i}(t)$ and $v_{e,i}(t)$ are the sliding and the entraining velocities (m/s) of $i^{th}$ meshing tooth pair; $w_n$ is the unit normal load (N/mm); $S_{avg}$ is the averaged surface roughness (μm), and $\eta_M$ is the dynamic viscosity of the oil entering the gear contact.

Xu and Kahraman [11-12] recently proposed yet another friction formula (designated as Model III) that is obtained by using a non-Newtonian, thermal EHL formulation. The proposed empirical sliding friction expression (for the $i^{th}$ meshing tooth pair), as based on non-Newtonian thermal EHL theory [12-13], is modified in our work to incorporate a reversal in the direction of the friction force at the pitch point as follows:

$$\mu_{Xi}(t) = e^{f\left(SR_i(t), P_{hi}(t), \eta_M, S_{avg}\right)} P_{hi}^{b_2} \left|SR_i(t)\right|^{b_3}$$
$$\cdot V_{ei}^{b_6}(t) \eta_M^{b_7} R_i^{b_8}(t) \cdot \mathrm{sgn}\left[\mathrm{mod}(\Omega_p r_{bp} t, \lambda) + (n-i)\lambda - L_{AP}\right]$$
$$f\left(SR_i(t), P_{hi}(t), \eta_M, S_{avg}\right) = b_1 + b_4 \left|SR_i(t)\right| P_{hi}(t) \log_{10}(\eta_M)$$
$$+ b_5 e^{-\left|SR_i(t)\right| P_{hi}(t) \log_{10}(\eta_M)} + b_9 e^{S_{avg}}$$
$$i = 0, \ \ldots, \ n. \tag{12a,b}$$

where $P_h(t)$ is the maximum Hertzian pressure (GPa); $SR(t)$ is the dimensionless slide-to-roll ratio; $V_e(t)$ is the oil entraining velocity (m/s) and $R$ is the effective radius of curvature (m). The empirical coefficients $b_j$ (in consistent units) are suggested by Xu and given in reference [12].

Duan and Singh [14] developed a smoothened Coulomb model for dry friction in torsional dampers; it could be applied to gears to obtain a smooth transition at the pitch point and we designate this as Model IV. Xu [12] conducted a series of friction measurements on a ball-on-disk test machine and measured the $\mu(t)$ values as a function of $SR$; these results resemble the smoothening function reported by Duan and Singh [14] near the pitch point ($SR$ = 0) especially at very low speeds (boundary lubrication conditions). By denoting the periodic displacement of $i^{th}$ meshing tooth pair as $x_i(t) = \mathrm{mod}(\Omega_p r_{bp} t, \lambda) + (n-i)\lambda - L_{AP}$, a smoothening function could be used in place of the discontinuous Coulomb friction. The arc-tangent type function is proposed as follows though one could also use other functions [8]:

$$\mu_{Si}(t) = \frac{2\mu_{avg}}{\pi} \arctan\left[\Phi x_i(t)\right] + \frac{2\mu_{avg}\Phi x_i(t)}{\pi\left[1 + \Phi^2 x_i^2(t)\right]} \quad i = 0 \ \ldots \ n \tag{13}$$

Here, the regularizing factor Φ is adjusted to suit the need of smoothening requirement. A higher value of Φ corresponds to a steeper slope at the pitch point.

**Table 1:** Parameters of example gear pair: NASA spur gear pair with unity ratio

| *Parameter/property* | *Pinion/Gear* |
|---|---|
| Number of teeth | 28 |
| Diametral pitch, $in^{-1}$ | 8 |
| Pressure angle, deg | 20 |
| Outside diameter, in | 3.738 |
| Root diameter, in | 3.139 |
| Face width, in | 0.25 |
| Tooth thickness, in | 0.191 |
| Center distance, in | 3.5 |
| Elastic modulus, psi | $30\times10^6$ |
| Density, $lb\cdot s^{-2}\cdot in^{-4}$ | $7.3\times10^{-4}$ |
| Bearing stiffness (LOA and OLOA), lb/in | $20\times10^6$ |

A case study is conducted here by using a non-unity ratio spur gear pair with parameters of Table 1. Figure 2 compares four alternate friction models on a normalized basis. The curves between $0 \le t/t_c < 1$ are defined for pair # 1 and those between $1 \le t/t_c < 2$ are defined for pair # 0. Discontinuities exist near the pitch point for Models I and II, and these may serve as artificial excitations to the OLOA dynamics. Also, smooth transitions are observed for Models III and IV corresponding to the EHL lubrication condition.

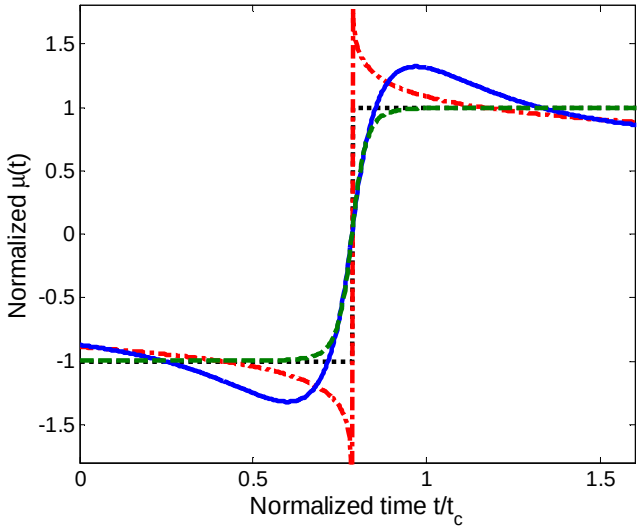


**Figure 2**: Comparison of normalized friction models. Key: ..... Model I; - . - Model II [9]; ——— Model III [11]; – – Model IV.

Figure 3 compares the combined normal loads and friction force time histories, as predicted by four friction models, given $T_p$ = 56.5 N-m (500 lb-in) and $\Omega_p$ = 4875 RPM. Note that while Fig. 2 illustrates $\mu(t)$ for each meshing tooth pair the friction forces of Fig. 3 include the contributions from both (all) meshing tooth pairs. Though alternate friction formulations dictate the dynamic friction force profiles, they have negligible effect on the normal loads.

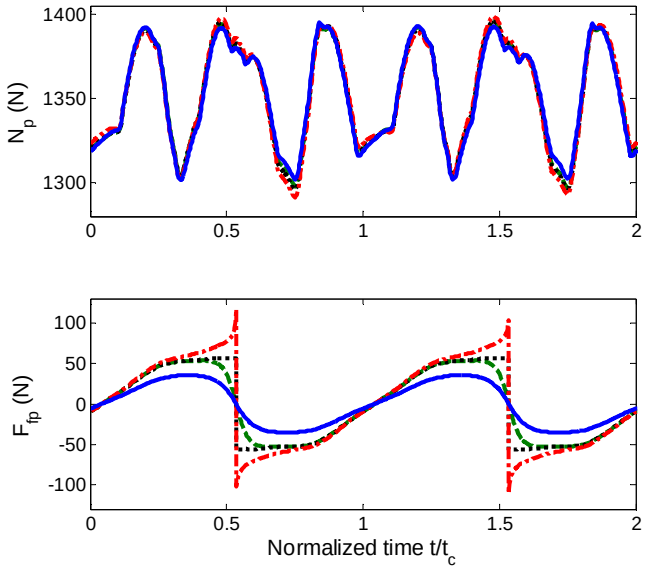


**Figure 3**: Combined normal load and friction force time histories predicted by alternate friction models given $T_p$ = 56.5 N-m (500 lb-in) and $\Omega_p$ = 4875 RPM. Key: ..... Model I; - - - Model II; ——— Model III; – – – Model IV.

Predicted normal load and friction force time histories (with Model III) are also validated using the benchmark friction measurements made by Rebbechi et al. [10]. Results are shown in Fig. 4. Based on the comparison, $\mu$ is estimated to be about 0.004 since it was not given in the experimental study. Here, we have made the periodic LTV definitions of meshing tooth pairs # 0 and 1 to be consistent with those of measurements, where meshing tooth pairs A and B are labeled in a continuous manner. Our predictions match well with measurements made by Rebbechi et al. [10].

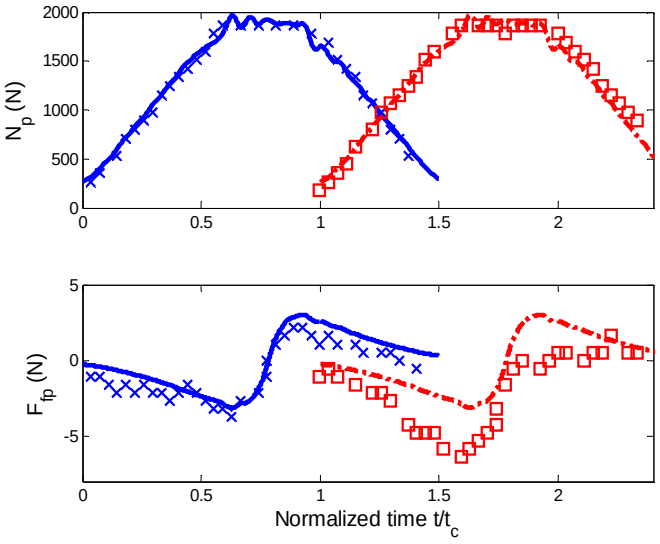


**Figure 4:** Validation of predicted normal load and sliding friction force: (a) at $T_p$ = 79.1 N-m (700 lb-in) and $\Omega_p$ = 800 RPM; (b) at $T_p$ = 79.1 N-m (700 lb-in) and $\Omega_p$ = 4000 RPM. Key: ——— prediction of tooth pair A with Model III; - - - prediction of tooth pair B with Model III; X measurement of tooth pair A [10]; □ measurement of tooth pair B [10].

## 4 INTERACTIONS BETWEEN TOOTH MODIFICATION AND SLIDING FRICTION

Application of tip relief is a well-established design practice that avoids contacts at the corners. Harris [15] developed this approach and Niemann [16] suggested two design approaches named as 'long' and 'short' relief, respectively. More specifically, the short relief gives a smooth transmission error curve at no load, while the long relief avoids corner contact at the peak load. Since such operational conditions occur infrequently, Munro [17] proposed an intermediate (medium) relief to yield a smooth transmission error curve at 75% of the peak design load. Such design calculations, however, ignore the influence of sliding friction, which might become dominant under lower speeds and/or high loads [1-3]. A case study is conducted next which would examine interactions between tip relief and sliding friction.

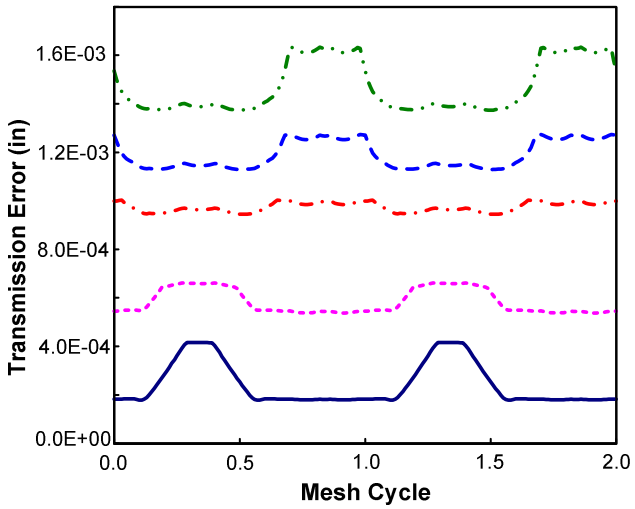


**Figure 5:** Harris map (STE) of long relief. Key: ———,100 (lb-in); ·····,300; - · - , 550; – – , 700; - · · - , 900.

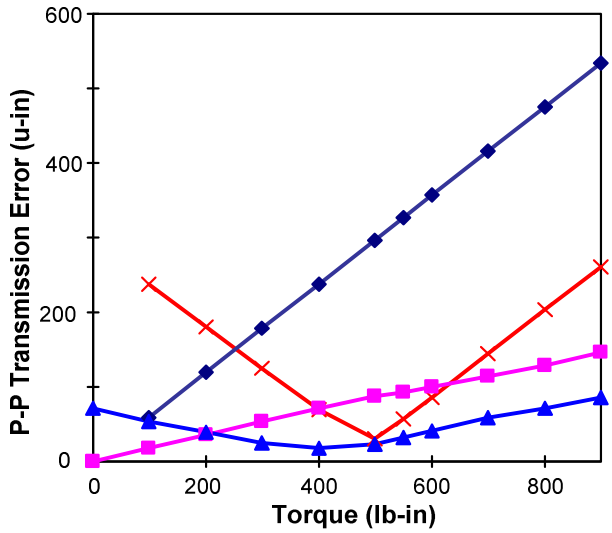


**Figure 6:** Transmission errors (p-p) vs. torque. Optimal load for short relief = 0; optimal load (75% of peak load) for medium relief = 400 lb-in; peak load for long relief = 550 lb-in. Key: ◆———◆, perfect involute; ■———■, short relief; ▲———▲, medium relief; ×———×, long relief.

Figure 5 shows the Harris map of predicted static transmission error (STE) for the long relief scheme (Table 1). Similar maps are also obtained for schemes including perfect involute, short relief and medium relief. Results are summarized in Fig. 6 in terms of peak-to-peak (p-p) STE as a function of the pinion torque. For the perfect involute case (without tip relief), the STE grows monotonically with load. The short tip relief is designed for light loads (0 lb-in). Its STE also increases with torque but the p-p variation is significantly reduced as compared to the perfect involute case. For long tip relief, the minimum p-p STE is obtained at the peak load around 550 lb-in. Away from the optimal load, the p-p STE grows with a slope similar to that of the perfect involute case. Finally, when the medium tip relief [17] is applied, minimum p-p STE is obtained at 75% of the peak load, i.e. $T_p \approx 400$ lb-in. Also the growth rate of STE away from the optimal load is lower when compared to the long relief case.

Realistic time-varying stiffness functions are calculated using a FE/CM code, External2D [18], at the nominal operational torque $T_p$. The effective stiffness function of the $i^{th}$ meshing tooth pair, as given earlier in Eq. (3), is defined as follows, where $N_i(t)$ and $\Theta_p(t)$ are the static normal load and pinion rotation obtained from FE/CM analysis.

$$k_i(t) = \frac{N_i(t)}{r_{bp}\Theta_p(t)}, \quad i = 0 \ldots \; n = \text{floor}(\sigma) \tag{14}$$

Due to the system periodicity, expanded stiffness function $k_i(t)$ of the $i^{th}$ meshing tooth pair is calculated at any time instant $t$ as: $k_i(t) = k[(n-i)t_c + \text{mod}(t, t_c)]$, $i = 0, \ldots n$. The stiffness function $k(t)$ for a single tooth pair rolling through the entire meshing process is obtained by following the contact tooth pair for $n = \text{ceil}(\sigma)$ number of mesh cycles. Effective $k(t)$ are calculated for four tip relief cases as illustrated in Fig. 7. Since the $k(t)$ profiles are weakly sensitive to $T_p$, only one set of results at $T_p = 400$ lb-in are shown over two mesh cycles. Observe that applying tip relief significantly changes the $k(t)$ profile of perfect involute gear; also the short and medium relief cases have reduced effective contact ratios.

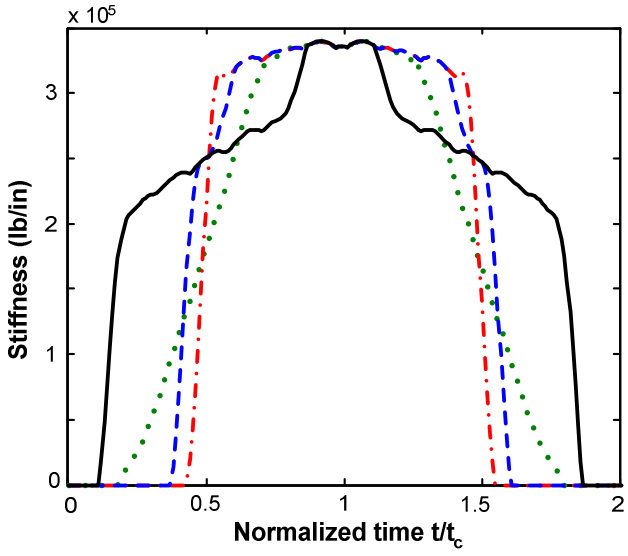


**Figure 7:** Stiffness functions of a single mesh tooth pair under $T_p = 400$ lb-in. Key: ——, perfect involute; – – ,short relief; – · – ,medium relief; ····· , long relief.

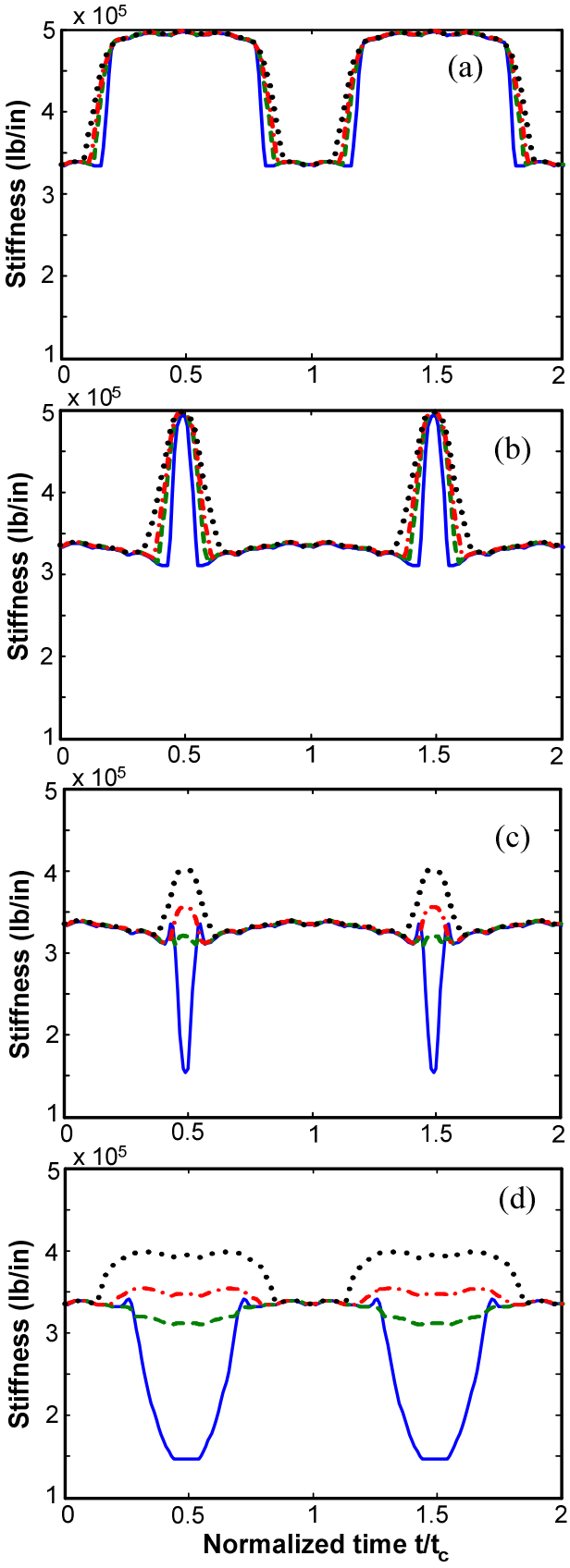


**Figure 8:** Combined tooth stiffness functions of the gear pair with long relief. Key: —— $T_p = 100$ lb-in; – – $T_p = 400$ lb-in; – · – $T_p = 550$ lb-in; ····· $T_p = 900$ lb-in.

For the example case with ceil($\sigma$) = 2, both meshing tooth pairs contribute to the overall mesh stiffness. Figure 8 shows the combined $k(t)$ over two mesh cycles at four loading conditions as following: light load ($T_p$ = 100 lb-in); optimal load of medium relief ($T_p$ = 400 lb-in); peak load of long relief ($T_p$ = 550 lb-in) and high load ($T_p$ = 900 lb-in). Observe that combined $k(t)$ of perfect involute gear pair of Fig. 8(a) follows a rectangular pattern, which is insensitive to a variation in the mean torque. For the short relief case of Fig. 8(b), high spikes are observed during the regions when two meshing tooth pairs are in contact; also, the profiles are insensitive to variations in the mean torque. On the other hand, for medium or long tip relief case, the combined stiffness function varies significantly with the mean torque; minimum p-p variations are obtained at their individual optimal loads, where the corner contact is minimized.

Using the MDOF spur gear model, dynamic studies are conducted for the example case at $T_p$ = 400 lb-in corresponding to the "optimal" case of medium relief case. Since the dynamic response is found to be insensitive to the dynamic coefficient of friction, a simplified Coulomb friction model of Eq. (10) is utilized with its magnitude estimated by a time-average of Benedict and Kelley model [9]. Equations (6-9) show that the combined normal loads $\Sigma N_i$ and friction forces $\Sigma F_{fi}$ dominate the LOA and OLOA dynamics, respectively.

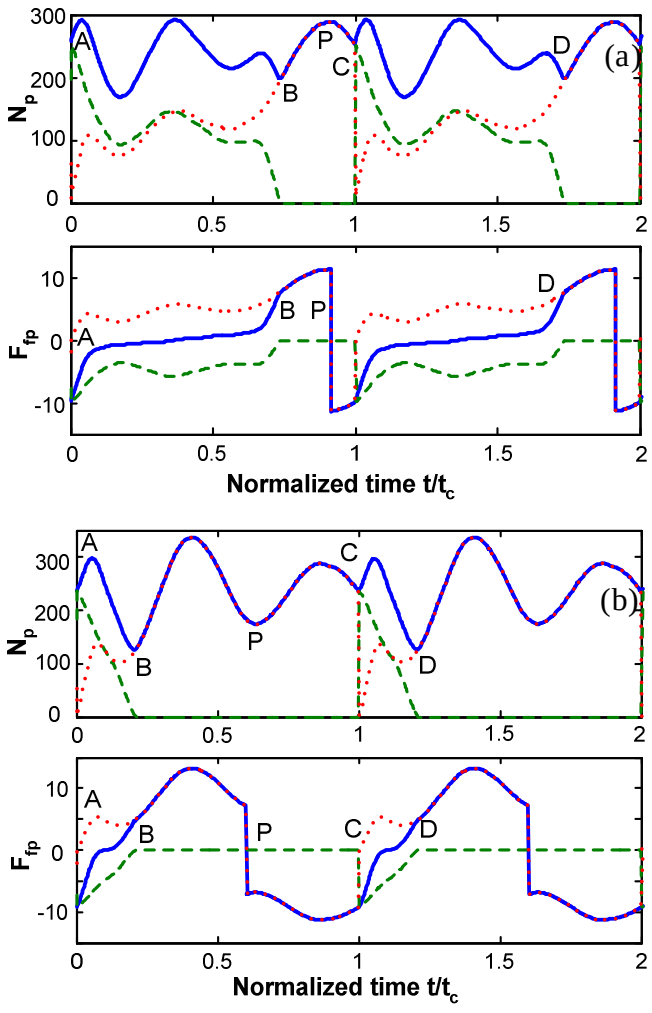


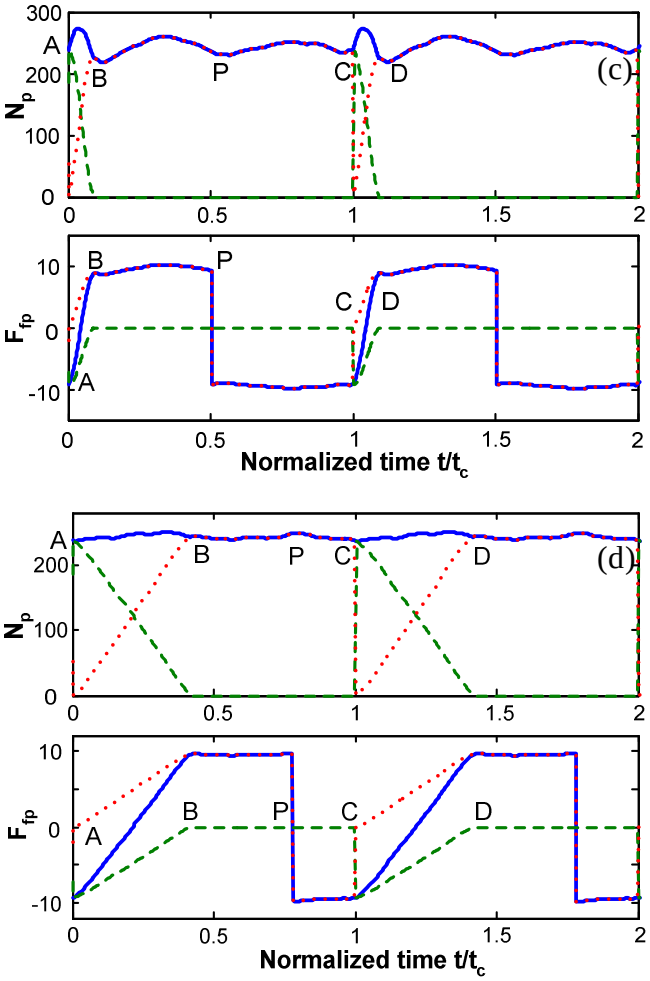


**Figure 9:** Dynamic normal loads $N_p$ and friction forces $F_{fp}$ predicted at 400 lb-in, 4875 RPM and 140 ℉ with $t_c$ = 0.44 ms: (a) perfect involute; (b) short relief; (c) medium relief; (d) long relief. Key: ——, combined; ……, tooth pair #0; – – , tooth pair #1.

The force profiles of tooth pairs #0 and #1 are obtained over two continuous meshing cycles as shown in Fig. 9(a-d) for four tip relief cases, respectively. Recall the earlier definitions of points A (initial contact point), B (LPSTC), P (pitch point), C (HPSTC) and D (ending point) in Fig. 1(a). Observe the following: (1) the perfect involute and the long relief cases have longer double-tooth-contact regions (within AB or CD) compared with other two cases due to higher effective contact ratios. (2) Corner contacts are observed at A, B, C and D for combined pinion normal force $\Sigma N_{pi}$ of perfect involute gear. These are effectively reduced by applying various amounts of tip relief. (3) The p-p variation of $\Sigma N_{pi}$ is minimized for the medium and long tip relief cases at 400 lb-in. This could be explained by an out-of-phase relationship of $N_{p1}$ and $N_{p2}$ between A and B (or C and D) due to the tip relief. On the other hand, $N_{p1}$ and $N_{p2}$ of the perfect involute case tend to be in-phase with each other; thus we observe an amplification of $\Sigma N_{pi}$ in the double-tooth-contact regions. (4) Although the p-p variation of combined pinion friction force $\Sigma F_{fpi}$ tends to be dictated by the magnitude of normal loads $\Sigma N_{pi}$ around the pitch point P, its dynamic transitions during the double-tooth-

contact regions (AB, CD, etc.) is governed by the phase relationship between $F_{fp1}$ and $F_{fp2}$, which tends to be opposite to the phase between $N_{p1}$ and $N_{p2}$ due to sliding friction, as formulated by Eq. (10).

Consequently, for the involute gear where $N_{p1}$ and $N_{p2}$ amplify the dynamic oscillations, $F_{fp1}$ and $F_{fp2}$ are out-of-phase. Thus the combined friction forces are minimized within the double-tooth-contact regions. Meanwhile, when medium or long tip relief is applied to avoid corner contacts, such as in Figs. 9(c-d), $F_{fp1}$ and $F_{fp2}$ are in-phase and significantly amplify $\Sigma F_{fpi}$ within the same regions. The out-of-phase relationship between $N_{pi}$ and $F_{fpi}$ explains why the tip relief (designed to minimize the STE) would tend to increase the friction force excitation.

Next, interactions between tip relief and sliding friction are examined using bearing forces $F_{pBx}(t) = -2\zeta_{pBx}\sqrt{K_{pBx}m_p}\,\dot{x}_p(t) - K_{pBx}x_p(t)$ and $F_{pBy}(t) = -2\zeta_{pBy}\sqrt{K_{pBy}m_p}\,\dot{y}_p(t) - K_{pBy}y_p(t)$ in the LOA and OLOA directions and the dynamic transmission errors (DTE) $\delta(t) = r_{bp}\theta_p(t) - r_{bg}\theta_g(t) + x_p(t) - x_g(t)$. These are obtained by numerically integrating the governing equations for various tip relief cases. Figure 10 shows typical dynamic responses at $T_p$ = 400 lb-in in time domain. Note that the DTE and $F_{pBx}$ share similar patterns (despite a 180° phase difference) since the translations $x(t)$ are dominant at the bearings. Note that the dynamic components of $F_{pBx}$ are superposed on a compressive mean load, while the dynamic components of $F_{pBy}$ are associated with a periodic change in direction.

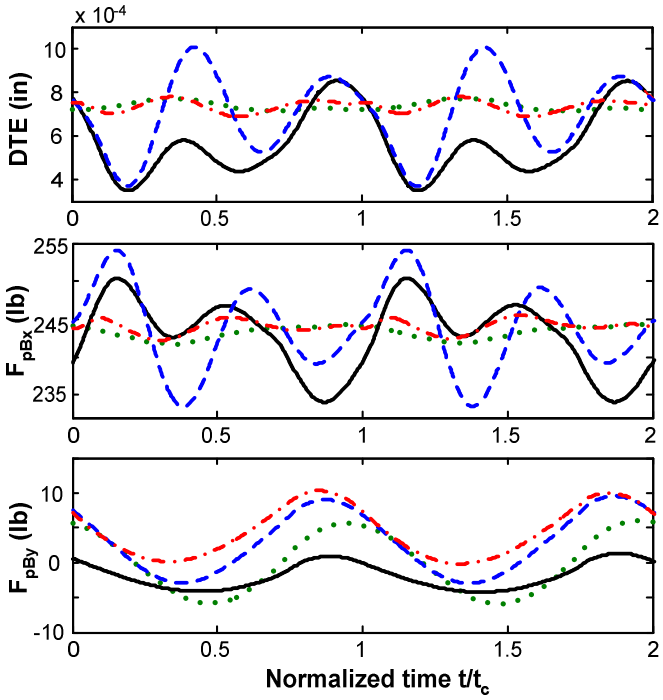


**Figure 10:** DTE, LOA and OLOA bearing forces predicted at 400 lb-in, 4875 RPM and 140 ℉ with $t_c$ = 0.44 ms: Key: ——— perfect involute; – – – short relief; – · – · – medium relief; ..... long relief.

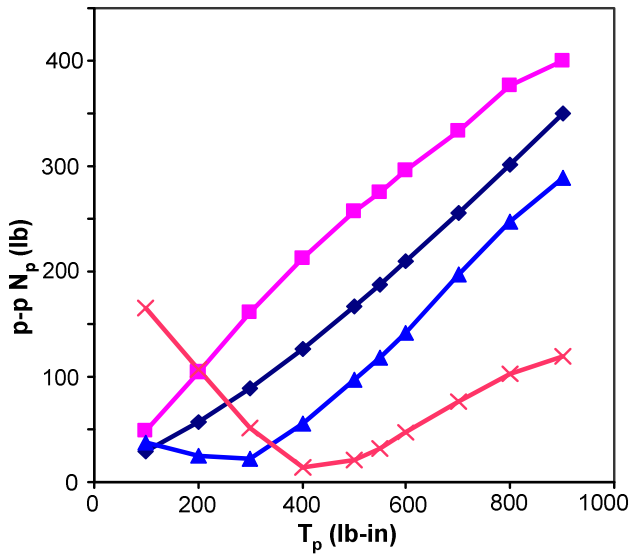


**Figure 11:** Combined dynamic normal loads (p-p). Key: ◆———◆, perfect involute; ■———■, short relief; ▲———▲, medium relief; ×———×, long relief.

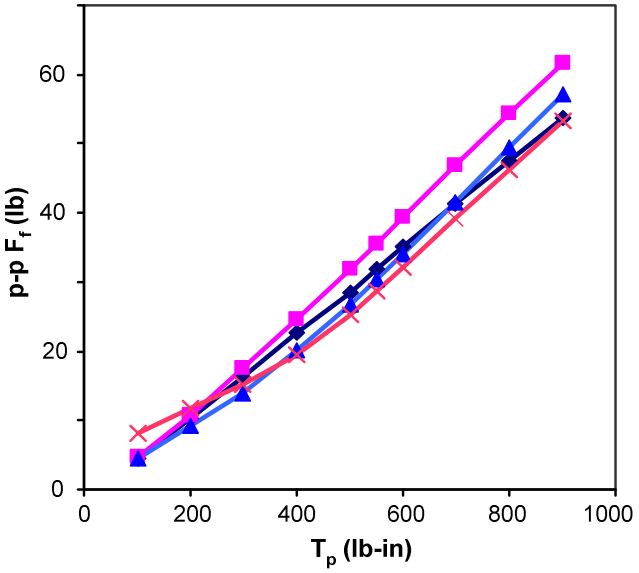


**Figure 12:** Combined dynamic friction forces (p-p). Key: ◆———◆, perfect involute; ■———■, short relief; ▲———▲, medium relief; ×———×, long relief.

Since the dynamic bearing forces play an important role in structure-borne noise and vibration, parametric studies are conducted on a peak-to-peak (p-p) basis for all dynamic responses. Figures 11 and 12 compare the p-p combined normal loads $\Sigma N_{pi}$ and friction forces $\Sigma F_{fpi}$ as functions of the mean torque $T_p$. Observe in Fig. 11 that minimum p-p $\Sigma N_{pi}$ are obtained at 300 and 400 lb-in for medium and long relief cases, respectively. Compared with the p-p STE distribution in Fig. 6, the "optimal" torques are shifted to lower values due to dynamic effects. The p-p friction forces $\Sigma F_{fpi}$ of Fig. 12, however, remain almost the same for all loading conditions. This is consistent with the observation of Fig. 9 that the p-p combined friction force is dictated by the magnitude of normal loads $\Sigma N_{pi}$ around the pitch point $P$.

Figure 13 show the predicted p-p LOA bearing forces $F_{pBx}$ as functions of $T_p$. Similar patters are observed for both $F_{pBx}$ and predicted DTE (results not shown due to similarity) as compared with the $\Sigma N_{pi}$ of Fig. 11. This implies that the combined dynamic normal loads tend to influence DTE as well as the LOA dynamics. However, for the OLOA bearing forces $F_{pBy}$ illustrated in Fig. 14, significant differences are observed as compared to the friction force $\Sigma F_{fpi}$ of Fig. 12. The perfect involute gear tends to have the minimum p-p oscillations because of the cancellation of $F_{fp1}$ and $F_{fp2}$ in the double-tooth-contact regions. When the tip relief is applied, the p-p dynamic bearing forces $F_{pBy}$ is enhances due to the in-phase relationship between $F_{fp1}$ and $F_{fp2}$.

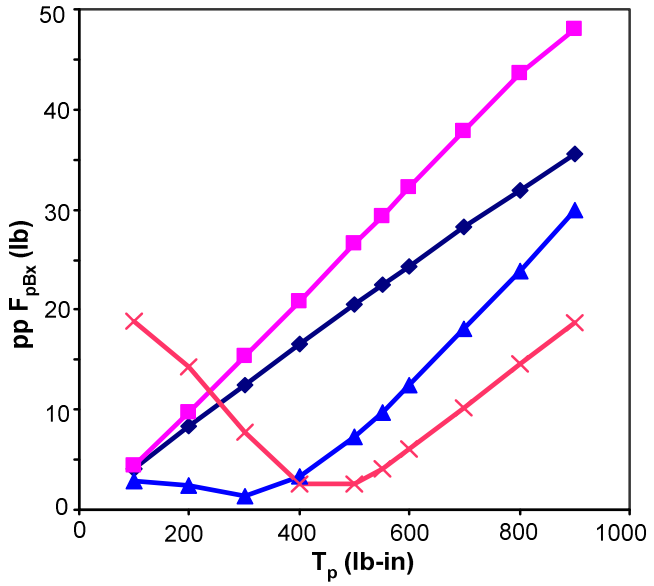


**Figure 13:** LOA pinion bearing force (p-p). Key: ◆, perfect involute; ■, short relief; ▲, medium relief; ✕, long relief.

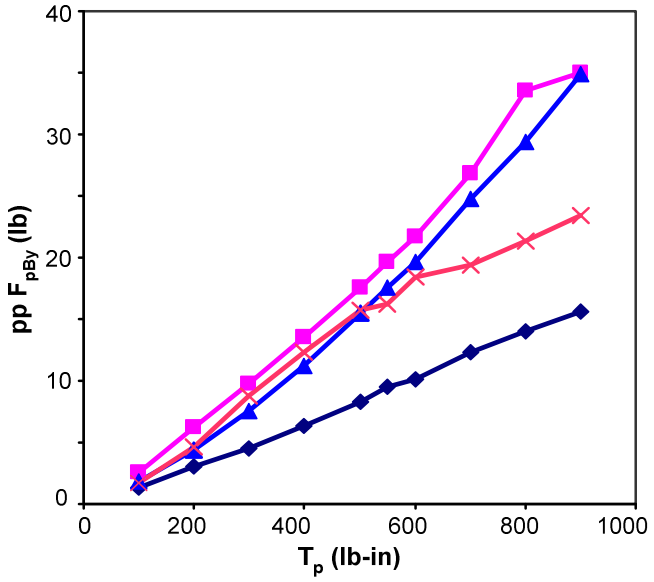


**Figure 14:** OLOA pinion bearing force (p-p). Key: ◆, perfect involute; ■, short relief; ▲, medium relief; ✕, long relief.

## 5 CONCLUSION

Figure 15 illustrates the ratio of p-p $F_{pBy}$ to p-p $F_{pBx}$, as a function of $T_p$. The significance of sliding friction is clearly illustrated as follows. Away from the "optimal" load, dynamic bearing forces in the OLOA direction are only as much as 30-50% of the oscillatory forces in the LOA direction. When the STE (and thus the variation in the normal loads) has been minimized by the application of tip relief, the resultant dynamic bearing forces in the LOA direction are greatly reduced. Conversely, the OLOA dynamic bearing forces are efficiently amplified due to the out-of-phase relationship between $N_{pi}$ and $F_{fpi}$. Thus, the OLOA bearing force due to the friction force could grow 6 times higher than the comparable forces that would be induced by STE alone. Thus, in order to effectively control the structure-borne noise of a spur gear system, one must consider sliding friction as a key source and attempt to minimize dynamic interactions between tip relief and sliding friction.

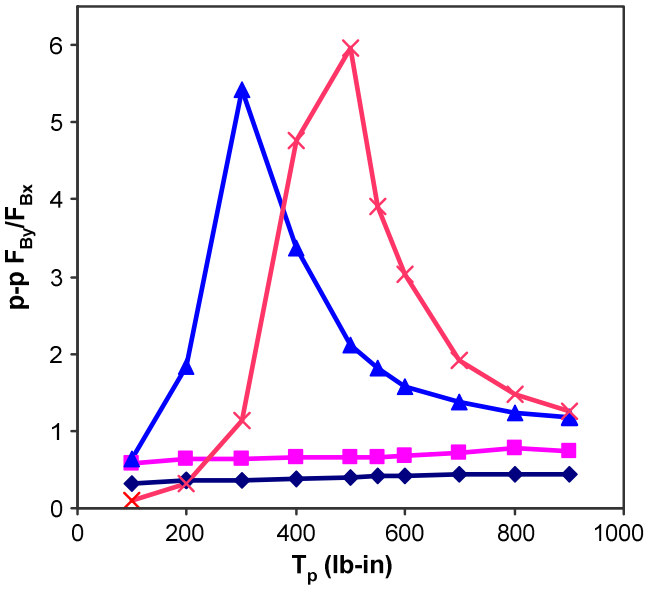


**Figure 15:** Pinion bearing force ratio $F_{pBy}/F_{pBx}$ (p-p). Key: ◆, perfect involute; ■, short relief; ▲, medium relief; ✕, long relief.

In order to quantify the amplification of OLOA bearing force due to interactions between tip relief and sliding friction, two metrics are proposed by calculating the ratios $F_{pBx}/\Sigma N_{pi}$ and $F_{pBy}/\Sigma F_{pfi}$ as a function of the mean torque $T_p$. Figures 16 (a-b) illustrate the results with consistent scales. Observe that the $F_{pBx}/\Sigma N_{pi}$ ratios (in the LOA direction) remain almost constant between 0.05-0.2 over the entire torque range, while applying tip relief significantly alters the $F_{pBy}/\Sigma F_{pfi}$ ratios (in the OLOA direction). For instance, a peak is observed for the long tip relief case around the "optimal" load, implying that an amplification due to the sliding friction takes place. Further work is needed to examine the dynamic design implications in the context of structure-borne and radiated noise.

## 6 ACKNOWLEDGMENTS

We gratefully acknowledge support from the U.S. Army Research Office (grant number DAAD19-02-1-0334, from

2002 to 2005). Dr. S. Vijayakar and Dr. R. Gunda (Advanced Numerical Solutions, Inc.) are thanked for providing access to the Calyx gear analysis software. Finally, we acknowledge Prof. G. Pavic (INSA Lyon, France) for his support for the first author during the preparation of this paper.

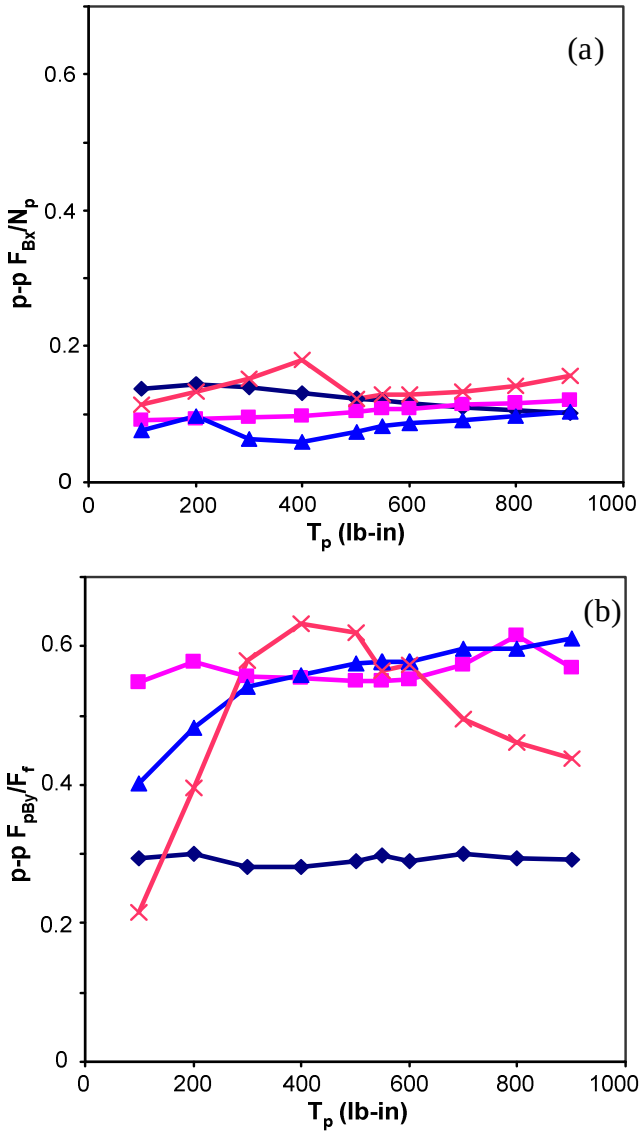


**Figure 16:** Pinion bearing force ratios (p-p): (a) $F_{pBx}/N_p$. (b) $F_{pBy}/F_{pf}$. Key: ◆, perfect involute; ■, short relief; ▲, medium relief; ×, long relief.

## 7 REFERENCES

[1] Vaishya, M. and Singh, R., 2003, "Strategies for Modeling Friction in Gear Dynamics," *ASME J. Mech. Des.*, **125**, pp. 383-393.

[2] Vaishya, M. and Singh, R., 2001, "Analysis of Periodically Varying Gear Mesh Systems with Coulomb Friction using Floquet Theory," *J. Sound Vib.*, **243**(3), pp. 525-545.

[3] Vaishya, M. and Singh, R., 2001, "Sliding Friction-Induced Non-Linearity and Parametric Effects in Gear Dynamics," *J. Sound Vib.*, **248**(4), pp. 671-694.

[4] Houser D. R., Vaishya M. and Sorenson J. D., 2001, "Vibro-acoustic Effects of Friction in Gears: An Experimental Investigation," *SAE* paper No. 2001-01-1516.

[5] Velex P. and Cahouet V., 2000, "Experimental and Numerical Investigations on the Influence of Tooth Friction in Spur and Helical Gear Dynamics," *ASME J. Mech. Des.*, **122** (4), pp. 515-522.

[6] Velex, P. and Sainsot, P., 2002, "An Analytical Study of Tooth Friction Excitations in Spur and Helical Gears," *Mech. Mach. Theory*, **37**, pp. 641-658.

[7] Lundvall, O., Strömberg, N. and Klarbring, A., 2004, "A Flexible Multi-Body Approach for Frictional Contact in Spur Gears," *J. Sound Vib.*, **278**(3), pp. 479-499.

[8] He, S., Gunda, R. and Singh, R., 2007, "Effect of Sliding Friction on the Dynamics of Spur Gear Pair with Realistic Time-Varying Stiffness," *J. Sound Vib.*, **301**, pp. 927-949.

[9] Benedict, G. H. and Kelley, B. W., 1961, "Instantaneous Coefficients of Gear Tooth Friction," *Trans. American Society of Lubrication Engineers*, **4**, pp. 59-70.

[10] Rebbechi, B., Oswald, F. B. and Townsend, D. P., 1996, "Measurement of Gear Tooth Dynamic Friction," *ASME PTG Conf. Proc. DE*, **88**, pp. 355-363.

[11] Xu, H., Kahraman, A., Anderson, N. E. and Maddock, D. G., 2007, "Prediction of Mechanical Efficiency of Parallel-Axis Gear Pairs," *ASME J. Mech. Des.*, **129**, pp. 58-68.

[12] Xu, H., 2007, "Development of a Generalized Mechanical Efficiency Prediction Methodology," PhD Dissertation (Advisor: A. Kahraman), The Ohio State University.

[13] Hamrock, B. J. and Dowson, D., 1977, "Isothermal Elastohydrodynamic Lubrication of Point Contacts, Part III – Fully Flooded Results," *J. Lubrication Tech.*, **99**(2), pp. 264-276.

[14] Duan, C. and Singh, R., 2006, "Dynamics of a 3DOF Torsional System with a Dry Friction Controlled Path," *J. Sound Vib.*, **289**(4-5), pp. 657-688.

[15] Harris, S., 1958, "Dynamic Loads on the Teeth of Spur Gears," *Proc IMechE*, **172**(2), pp. 87.

[16] Niemann, G. and Baethge, J., 1970, "Transmission Error Tooth Stiffness, and Noise of Parallel Axis Gears," *VDIZ* 112 (4).

[17] Munro, R. G., 1990, "Optimum Profile Relief and Transmission Error in Spur Gears," *Proc IMechE*, Cambridge, England, 9-11 Apr., pp. 35-42.

[18] External2D (CALYX), ANSOL Inc., Hilliard, OH.

[19] AGMA Information Sheet 925-A03, 2003, "Effect of Lubrication on Gear Surface Distress".

[20] Singh, R., 2005, "Dynamic Analysis of Sliding Friction in Rotorcraft Geared Systems," technical report submitted to the Army Research Office, grant number DAAD19-02-1-0334.